Chapter 2

Experimental Facilities, Equipment and Apparatus

2.1 Stability Wind Tunnel

The Virginia Tech Stability Wind tunnel is a continuous, closed jet, single return, subsonic wind tunnel with six foot cross section interchangeable test sections. Each test section is 24 feet long. The tunnel is powered by a 600 HP D.C. motor driving a 14 foot propeller [4]. Surface flow experiments on DARPA2 model has been performed in $6' \times 6'$ square test section. In this configuration, a maximum speed of 275 ft/s and a Reynolds number up to 1.66×10^6 per foot can be obtained.

Tunnel speed is regulated by a custom designed Emerson VIP ES-6600 SCR Drive. This drive system eliminates all the cyclic unsteadiness in tunnel velocities and turbulence inducing vibrations inherent with older systems. The Stability Tunnel has a low turbulence intensity. The small-scale turbulence intensity is on the order of 0.03% or less depending on the tunnel speed. The unsteadiness due to large-scale pulsation of the fan was also found to be on the order of 0.03% [4].

The tunnel temperature is stabilized by the use of an air exchange tower. After a certain amount of operation time, tunnel temperature becomes equal to the outside temperature. Therefore the changes in the outside temperature directly effects the tunnel temperature. Since the hot-film sensors are sensitive to the ambient flow temperature as well as the

local skin-friction value, the changes in the free-stream temperature should be taken into account in the data acquisition and the reduction process.

Surface hot-film measurements on DARPA2 model have been performed in a slotted-wall test section with 38% open air ratio. The main purpose for using the slotted-wall configuration in the experiments is to reduce the blockage effects typically encountered during testing at high angles of attack with large models. More information about the slotted wall configuration in the stability tunnel can be found in [14]. Figure 2.1 shows the top view of the Stability Wind Tunnel.

2.2 DyPPiR

Unsteady maneuvers have been performed by using the **Dy**namic **P**lunge, **Pi**tch and **R**oll actuator of the Virginia Tech Stability Wind Tunnel, also known as the *DyPPiR*. The DyPPiR was designed to provide the unique capability of performing general, high excursion, large scale, high Reynolds number, unsteady maneuvers [4]. The DyPPiR has three degrees of freedom: plunge with a range of ± 0.64 m measured from the tunnel centerline, pitch with a motion range of $\pm 45\,^\circ$ and roll with a range of $\pm 140\,^\circ$. For each degree of freedom, there is an independent 3000 psi hydraulic actuator which can move a maximum model load of 45 kg and 250 kg of hardware load at rates approaching 9 m/s in plunge and 120 $^\circ/s$ in pitch. The DyPPiR has also the capability of performing maneuvers around an arbitrary model center of rotation, which is important for obtaining the correct lateral velocities across the aircraft, missiles and submarines. The DyPPiR is computer controlled and in addition to traditional sinusoidal, ramp and snaking maneuvers, any pre-programmed *real* maneuver can be simulated, including time history effects. Previous tests have confirmed that the sting mount places the model far enough from the main DyPPiR strut to make strut interference negligible [3]. Figure 2.2 shows the DyPPiR installed in the stability wind tunnel. For DARPA2 experiments, besides unsteady maneuvers, the DyPPiR has also been used as a computer controlled model mount for the steady skin friction measurements. Due to a technical problem in the hydraulically powered roll actuator, a manually controlled dummy roll actuator has been built and used to change the roll angle of the model. This enabled a full $360\,^\circ$ coverage of the model roll orientation. The coordinate nomenclature for the DyPPiR and the model

is shown in figure 2.3: x is measured from the nose, ϕ is the circumferential location measured from the windward line of symmetry, z is the plunge ordinate, and α is the pitch angle and equivalently the model center of rotation angle of attack.

2.3 Data Acquisition System

The tunnel data acquisition system has been used for sampling the analog signals from each hot-film anemometer as well as recording tunnel dynamic pressure, static pressure and the tunnel temperature in steady and unsteady skin friction measurements. Since the tunnel data acquisition system is incorporated and synchronized with the DyPPiR control system, it has also been used for recording the plunge, pitch and roll command and feedback signals (voltage values). These values were converted to proper dimensional units by using a linear calibration routine which gave the location and the orientation of the model as a function of time.

The centerpiece of the system is an SCXI-1001 Mainframe from National Instruments. The mainframe allows for the installation of up to 12 SCXI modules which may perform any desired signal conditioning and sampling of the input signals. Currently four SCXI-1120D isolation modules are installed in the mainframe. Each of these modules allows isolation and amplification of 8 differential analog voltages with an input range of -10 to $+10$ volts. Each module multiplexes the 8 inputs which are read by a National Instruments AT-MIO-16-XE-10 Data Acquisition Card installed in the tunnel computer. This results in a total of 32 isolated differential analog input channels with an Analog to Digital conversion resolution of 16 bits. The software used for data acquisition is written using LabView 4.0 under the Windows NT environment.

2.4 Skin-Friction Measurement System

Hot-film sensors mounted on the surface of the DARPA2 model were used to measure steady and unsteady skin friction magnitudes in the experiments. Each hot-film sensor was connected to a constant temperature type anemometer. Hot-film sensors and the constant temperature anemometers were the same as the ones used by Wetzel [2] in his prolate spheroid study.

2.4.1 Hot-film Sensors

Theory of Operation

The thermal or hot-film sensor benefits from the fact that the heat transfer from a sufficiently small heated surface depends only on the flow characteristics in the viscous region of the boundary layer [15]. Due to the similarity between gradient transport of momentum and scalars (heat), the amount of heat transfer into the fluid gives a measure of the wall shear stress τ_w. The hot-film gauge consists of a thin metallic film positioned into a substrate. Usually the gauge forms one part of a Whetstone bridge in the anemometer circuit and an electric current is passed through the film in order to maintain it at constant temperature (if a constant temperature anemometer is used) as heat is continuously being transferred from the film to the moving fluid as well as to the film's substrate.

The ohmic (joule) heating in the device Q_j is transferred both to the fluid and to the surrounding substrate. This can be expressed as:

$$Q_j = Q_s + Q_f \tag{2.1}$$

where Q_f represents the average heat transferred to the fluid directly from the heated surface and indirectly through the heated portion of the substrate. Q_s represents the average heat lost irretrievably to the substrate.

The relationship between the heat transfer Q_f and the wall shear stress τ_w can be obtained by making an unheated starting length forced convection analysis from a single heated sensor [7]. It is assumed that the thermal boundary layer developed on the sensor is within the viscous sublayer of a pre-existing momentum boundary layer.

We start our derivation for the relationship between Q_f and τ_w with the thermal energy transport equation near the wall for locally two dimensional flow:

$$U\frac{\partial T}{\partial x} = \alpha\frac{\partial^2 T}{\partial y^2} \tag{2.2}$$

Here x is the streamwise coordinate and y represents the normal-to-wall coordinate. The temperature is T, U is the velocity in the x direction, and α is the thermal diffusivity. Since the flow upstream of the sensor is unheated, the incoming flow temperature is the same as the free-stream temperature T_∞. We assume the sensor length in the streamwise

direction is short enough so that the thermal boundary layer grows from the upstream edge of the sensor, but remains entirely within the near wall region. In the viscous sublayer, we can approximate U as:

$$U = \left(\frac{\partial U}{\partial y}\right)_w y \tag{2.3}$$

where $\left(\frac{\partial U}{\partial y}\right)_w$ is the mean velocity gradient at the wall and the shear stress at the wall is given by:

$$\tau_w = \mu \left(\frac{\partial U}{\partial y}\right)_w \tag{2.4}$$

Here μ is the dynamic viscosity of the fluid. By putting non-dimensional temperature $\tilde{T}$

$$\tilde{T} = \frac{T - T_w}{T_\infty - T_w} \tag{2.5}$$

into equation 2.2 and using equation 2.3, we will have:

$$\left(\frac{\partial U}{\partial y}\right)_w y \frac{\partial \tilde{T}}{\partial x} = \alpha \frac{\partial^2 \tilde{T}}{\partial y^2} \tag{2.6}$$

The boundary conditions for this problem in terms of $\tilde{T}$ would be:

$$\tilde{T} = 0 \qquad at \qquad y = 0 \tag{2.7}$$

$$\tilde{T} = 1 \qquad as \qquad y \to \infty \tag{2.8}$$

$$\tilde{T} = 1 \qquad at \qquad x = 0 \tag{2.9}$$

To reduce the partial differential equation given by 2.6 to an ordinary differential equation, we introduce the similarity parameter η defined as:

$$\eta = \frac{y \left(\frac{\partial U}{\partial y}\right)_w^{1/3}}{(3\alpha x)^{1/3}} \tag{2.10}$$

And the resulting ordinary differential equation would be:

$$\tilde{T}'' + \eta^2 \tilde{T}' = 0 \tag{2.11}$$

Boundary conditions for equation 2.11 in terms of η become:

$$\tilde{T} = 0 \qquad at \qquad \eta = 0 \tag{2.12}$$

$$\tilde{T} = 1 \qquad as \qquad \eta \to \infty \tag{2.13}$$

The solution of the ordinary differential equation can be obtained as:

$$\tilde{T} = M \int_0^{\eta} e^{-\eta^3/3}\, d\eta \tag{2.14}$$

where

$$M^{-1} = \int_0^{\infty} e^{-\eta^3/3}\, d\eta = \frac{1}{3}\Gamma\left(\frac{1}{3}\right) = 0.893 \tag{2.15}$$

The heat flux at the surface is given by:

$$q_w = -k\left(\frac{\partial T}{\partial y}\right)_w = -k(T_\infty - T_w)\left(\frac{\partial \tilde{T}}{\partial y}\right)_w \tag{2.16}$$

Here k is the thermal conductivity. By using equation 2.14 and the chain rule;

$$\frac{\partial \tilde{T}}{\partial y} = \frac{\partial \tilde{T}}{\partial \eta}\frac{\partial \eta}{\partial y} \tag{2.17}$$

we obtain q_w as:

$$q_w = Mk(T_\infty - T_w)\frac{\left(\frac{\partial U}{\partial y}\right)_w^{1/3}}{(3\alpha x)^{1/3}} \tag{2.18}$$

Assuming that we have a rectangular sensor of constant width w in the spanwise direction and length of l in the streamwise direction, we can obtain the average heat transfer rate Q_f by integrating q_w over w and l:

$$Q_f = w\int_0^l q_w\, dx = \frac{3}{2}Mk(T_w - T_\infty)\frac{\left(\frac{\partial U}{\partial y}\right)_w^{1/3}}{(3\alpha)^{1/3}} l^{2/3} \tag{2.19}$$

Then by definition mean film coefficient $\bar{h}$ would be equal to:

$$\bar{h} = \frac{Q_f}{(T_w - T_\infty)} = \frac{3}{2}Mklw\frac{\left(\frac{\partial U}{\partial y}\right)_w^{1/3}}{(3\alpha l)^{1/3}} \tag{2.20}$$

As can be seen from equation 2.20, $\bar{h}$ is directly proportional to $\left(\frac{\partial U}{\partial y}\right)_w^{1/3}$, thus the wall shear stress τ_w. All the other parameters are properties of the fluid and the sensor. T_w represents the temperature of the hot-film sensor and in case a constant temperature anemometer circuit is used, this temperature remains constant. In the ideal case, the free-stream temperature T_∞ can also be considered as constant although in most cases, especially in long experimental run periods, there may be considerable changes in the

flow temperature. (This issue and the effects of free-stream temperature change to the calibration of the hot-film sensors will be discussed in chapter 4).

If we assume that the heat transfer to the substrate is minimized by using isolation methods and negligible, then in equation 2.1, the joule heating Q_j will be equal to the heat transfer to the fluid Q_f. For the hot-film sensor, we can write the joule heating term as:

$$Q_j = Q_f = \frac{E^2}{R_w} \tag{2.21}$$

where E is the voltage value across the hot-film sensor, and R_w is the resistance of the hot-film sensor at its operating temperature T_w. Since T_w is constant for a constant temperature anemometer, then R_w will also be constant by considering the well-known equation:

$$R_w = R_c \left[1 + \alpha_R \left(T_w - T_c\right)\right] \tag{2.22}$$

In the above equation, R_c is the resistance of the hot-film in a known temperature T_c and α_R is the temperature coefficient of resistivity. By using equation 2.20 in accordance with the equation 2.21;

$$\frac{E^2}{T_w - T_\infty} \propto \tau_w^{1/3} \tag{2.23}$$

Therefore, after a proper calibration, one can determine the shear stress value τ_w by measuring E.

Specifications of the Hot-film Sensors used in the Experiments

To measure the skin-friction, hot-film sensors designed and documented by Simpson et al. [7] were used. Figure 2.4 shows the top view of a typical sensor. The hot-film sensors are made of Balco foil (70% nickel, 30% iron) with a nominal temperature coefficient of resistivity of $0.0051/\,^{\circ}C$ and are manufactured by the MINCO, Inc. The main sensing part of the sensor is a spiral of 5.1 mm in diameter which is approximately 0.23% of the model length. At the constant diameter section of the model, the sensor occupies $2.184\,^{\circ}$ of the model surface along the circumference. The foil sensor is bonded to a kapton substrate and the total sensor thickness is 0.0635 mm. Sensors are connected to the constant temperature anemometers by 22 AWG wires, which are soldered on the two tabs of the foil.

It should be noted that the hot-film sensors have been designed to measure only the magnitude of the skin-friction as described in Simpson et al. [7]. However, in his prolate spheroid study, Wetzel [2] detected a directional sensitivity of as much as ±5%. He reduced the directional sensitivity effects to less than 3% by mounting the sensors at 65 ° off the longitudinal line on the model surface. In this study, the sensor were placed parallel to the longitudinal line on the model surface. Wetzel [2] also showed that the sensors are incapable of resolving small scale turbulence structures due to the relatively large sensor size. The skin-friction magnitudes measured by the hot-film sensors are actually the values spatially-averaged over the sensing spiral part.

2.4.2 Constant Temperature Anemometers

The hot-film sensors were operated with Miller-type non-linearized constant temperature anemometers [16]. The original boards were modified by Wetzel [2] in the prolate spheroid study. For the Suboff tests, some further adjustments were made in order to increase the stability of the anemometers and to reduce the noise associated with the electronics. The main power supply was replaced with a new one that can supply sufficient amount of current to each anemometer at long run periods and at relatively high speeds. This change enabled the use of fifteen anemometers simultaneously during the tests without any power loss. Some of the op-amps in the anemometer circuits that were not functioning properly were replaced with the new ones and this reduced the noise level significantly. All the channels were grounded properly. Some of the current knobs were replaced with the new ones in order to increase the accuracy of setting the overheat ratio. Constant temperature anemometers had a bridge ratio of 60 and the hot-film sensors were operated at a nominal, but imprecisely set, overheat ratio of 1.10.

The frequency response of the Miller-type anemometers with the present hot-film sensors was determined to be approximately 200 Hz by Wetzel [2]. He used the method described in Wood [17] for finding the frequency response. While this frequency response is too low to measure the fluctuating turbulence quantities, it is high enough to resolve the time-history of the spatially-averaged skin-friction values in the unsteady maneuvers.

2.5 Wind Tunnel Model

The light weight Darpa2 model used in the experiments has a generic Suboff undersea vehicle geometry with a scaled length (L) of 2.24 m. The model has a bow region for $0.0 \leq (x/L) \leq 0.23$, a constant diameter region for $0.23 \leq (x/L) \leq 0.75$ and an afterbody (stern) region for $0.75 \leq (x/L) \leq 1.0$. The sail can be detached, resulting in the axi-symmetric configuration of the model which can be thought as a missile or to a certain extent an aircraft fuselage geometry. Geometric equations defining the shape of the model body and the sail are given in a DTRC (David Taylor Research Center) report [18]. The same equations are also included in Whitfield [13]. Figure 2.7 shows the computer generated image of the Suboff model by using these equations.

The geometry and the structural components of the model (except the ring assembly integrated to the model structure for moving the sail) are exactly the same as that of the Darpa2 model used in the force and moment measurements. Whitfield [13] gives an extensive description of the steps followed during the construction of the model and the structural details. The model is mainly made of composite materials. Between the inner and the outer carbon fiber layer, the vinyl foam and the aluminum bars having hollow square cross sections were placed on the constant diameter region of the model. On the nose and the stern regions, the honeycomb material was used to maintain the required curvature between the inner and the outer skin. The model weighs approximately 10 lbs. and has a high strength to weight ratio. This is an important property required in the unsteady maneuvers both for the structural integrity of the model and the performance of the DyPPiR.

The model is mounted to the DyPPiR with a light-weight composite sting which was also built for the Darpa2 force and moment measurements [13]. The last 15 cm of the stern region of the model was removed in order leave enough space for the sting and the wires coming from the sensors. The overall weight of the model with the composite sting is approximately 30 lbs.

2.5.1 Sensor Configuration and the Locations

Figure 2.8 shows the model geometry with the hot-film sensor locations. More sensors have been used near the body-sail junction region to resolve the complex structure of the

separated flow. Oil flow visualization pictures also have been used in order to determine the optimum sensor locations. A total number of 29 sensors were used on the Darpa2 Suboff body. Since only 15 anemometers could be run simultaneously, the sensors were separated into two groups each having 14 sensors. These sensor sets were labeled as *Sensor Set A* and *Sensor Set B*. Two ribbon cables, each carrying the wires connected to the sensors of each set, were used. These ribbon cables were lead outside of the model, to the carriage part of the DyPPiR where they were connected to the 15 BNC cables coming from the anemometers via gold plated pin-connectors. BNC cables were connected to a single female connector. Switching from one set of sensors to the other was simply done by connecting the pin-connector of the ribbon cable to be used to the single female connector. One sensor was individually connected directly to an anemometer and used as a *control sensor*. The data from this sensor were taken during all the runs regardless of the sensor set used in order to check the consistency of the measurements taken with different sensor groups in each model position and the orientation. The barebody measurements were performed by using the sensors of Set B and the individual control sensor located at certain positions on the long row (figure 2.8). The same sensors were used in the sail-on-side case throughout the whole circumferential locations. The remaining sensors (set A) were used near the sail region in order to resolve the flow structure. The nominal circumferential distance between the long and the short sensor row is $\Delta\phi = 11\,^\circ$. At some sensor locations, this distance vary by $\pm 1\,^\circ$. The uncertainty in the measurement of the peripheral distances is $\pm 0.44\,^\circ$. Table 2.1 gives the x/L location of each sensor. Wetzel [2] determined that to avoid the heating interference between adjacent and upstream sensors, they must be spaced at least 1.25 inches apart from each other. The minimum distance between the sensors used in the DARPA2 experiments is 1.32 inches which indicates the lack of any heating interface. For the sail-on-side configuration, the chordline of the sail is aligned with the circumferential location $\phi = 270\,^\circ$. At its maximum thickness location, the sail extends from $\phi = 262\,^\circ$ to $278\,^\circ$ and is placed between $x/L = 0.21$ and $x/L = 0.31$.

2.5.2 Sensor Mounting Strategy

Instead of directly mounting the sensors on the model surface, the hot-film sensors were first glued onto the cylindrical plugs made up of epoxy and the hardener as shown in

figure 2.5. The upper surface of the plugs (where the sensors were mounted) were shaped so that they match with the contour of model surface. The plugs have circular holes just beneath of the sensing spiral part of the sensors. These holes were filled with insulating foam to minimize the amount of the heat transfer into the model skin. Behind these, additional holes for the pressure taps were drilled in the plugs. At the sensor locations, hollow circular plastic cylinders were integrated to the model structure (figure 2.9). The sensor plugs were inserted into these holes (that had approximately the same diameters as the plugs) and were secured by using the hot-glue. This sensor installation strategy shown in figure 2.6 not only improves the surface quality in the vicinity of the sensors but also keeps the structural integrity of the model. The plug region where the sensor tabs were glued is inclined to the inner part of the model so that the wires that were soldered to the sensor tabs remain under the surface level. The resulting gap was filled with clay which was shaped to be levelled with the model surface.

2.5.3 Rotatable Ring

The sail was mounted on a movable ring integrated into the model structure and can be rotated and fixed to any desired circumferential location with 2° increments (figure 2.9). The ring is secured at the desired position by a set screw. Both in steady and unsteady testing, the skin friction magnitude distribution on the whole surface of the model with desired circumferential spacing can be obtained by using only one row of sensors on the model surface (note that the purpose of the second short sensor row shown in figure 2.8 is to resolve the skin-friction distribution around the sail in the x direction). The model is rotated with a certain roll angle in one direction while the sail is rotated in the opposite direction with the same amount. By this action, while changing the circumferential location of the row of sensors, the model geometry and the alignment relative to the free-stream for a specific pitch angle and sail location is kept constant. A small gap between the model and the sail has been kept in order the sail to be moved on top of the sensors without any contact. This gap has been sealed properly by using scotch tape and without giving any fillet effect for every roll angle before the data were taken.

2.5.4 Boundary Layer Trips

In order fix the transition location on the model and further guarantee a less Reynolds-number sensitive separation, trip posts of 0.76 mm high cylinders with 1.28 mm diameter, 2.5 mm spaced apart, were placed on the model nose part at $x/L = 0.10$. Two rows of the same trip posts were put on the lower and the upper surfaces of the sail in the spanwise direction. The rows were located 0.64 cm (measured on the surface) away from the leading edge of the sail. The same trips were used in the prolate spheroid study of Wetzel [2] and in the DARPA2 force and moment study of Whitfield [13].

2.6 Pressure Measurement System

Mean static pressures on the model surface were measured at 29 port locations listed in table 2.1. Each location is behind a hot-film sensor on the same sensor plug, and the distance between the pressure port and the hot-film sensor (measured from the center of the sensing spiral part) is approximately 0.2% of the overall model length (figure 2.5). Each pressure tap of each station was connected to a Scanivalve diaphragm (having 48 ports) through tygon tubing. These diaphragms were connected to a Scanivalve system (CTLR2P/S2-S6 Scanivalve Corp.) that has a 48 to 1 multiplexing. In order to reduce the length of the tygon tubing that connects each pressure tap with the scanivalve system, the housing of the scanivalve was placed inside the model and mounted on the sting by using cable tie-wraps. The pressures were sensed by two pressure transducers: a Setra 239 pressure transducer with a calibrated range of 0.0 to 15.0 inches of water was used to measure the free-stream dynamic pressure ($P_{0,\infty} - P_\infty$), and another Setra 239 pressure transducer with a calibrated range of -2.5 to 2.5 inches of water was used to measure the static pressure relative to the free-stream static pressure ($P - P_\infty$) at the pressure taps. Olcmen et al. [19] used an inclined manometer with a resolution of 0.01 inches to verify the calibration of the two pressure transducers. The total pressure $P_{0,\infty}$ and the free-stream static pressure P_∞ were measured by using the tunnel Pitot-static tube. The pressure coefficient C_p at each port is calculated by:

$$C_p = \frac{P - P_\infty}{P_{0,\infty} - P_\infty} \tag{2.24}$$

A data acquisition board (DT2801) installed in a PC-AT386 computer was used to acquire data from the pressure transducers at a sampling frequency of 1000 Hz. The data were sampled continuously for 3.0 seconds after a settling time of 10.0 seconds.

For the same pressure measurement system, the net uncertainty in C_p was reported as ± 0.018 by Olcmen et al. [19].

Table 2.1: Hot-film sensor locations (port number is the order of the sensors in x/L direction starting from the nose).

Port number	**Sensor Number**	**Sensor Set**	x/L
1	1	B	0.110
2	2	B	0.131
3	1	A	0.151
4	4	B	0.170
5	2	A	0.180
6	3	A	0.189
7	4	A	0.199
8	8	B	0.208
9	5	A	0.218
10	6	A	0.256
11	control	-	0.266
12	7	A	0.276
13	8	A	0.285
14	10	A	0.295
15	5	B	0.306
16	9	A	0.316
17	11	A	0.325
18	12	A	0.336
19	6	B	0.345
20	14	A	0.356
21	15	A	0.366
22	7	B	0.434
23	3	B	0.501
24	9	B	0.570
25	10	B	0.638
26	12	B	0.706
27	11	B	0.774
28	14	B	0.819
29	13	B	0.863

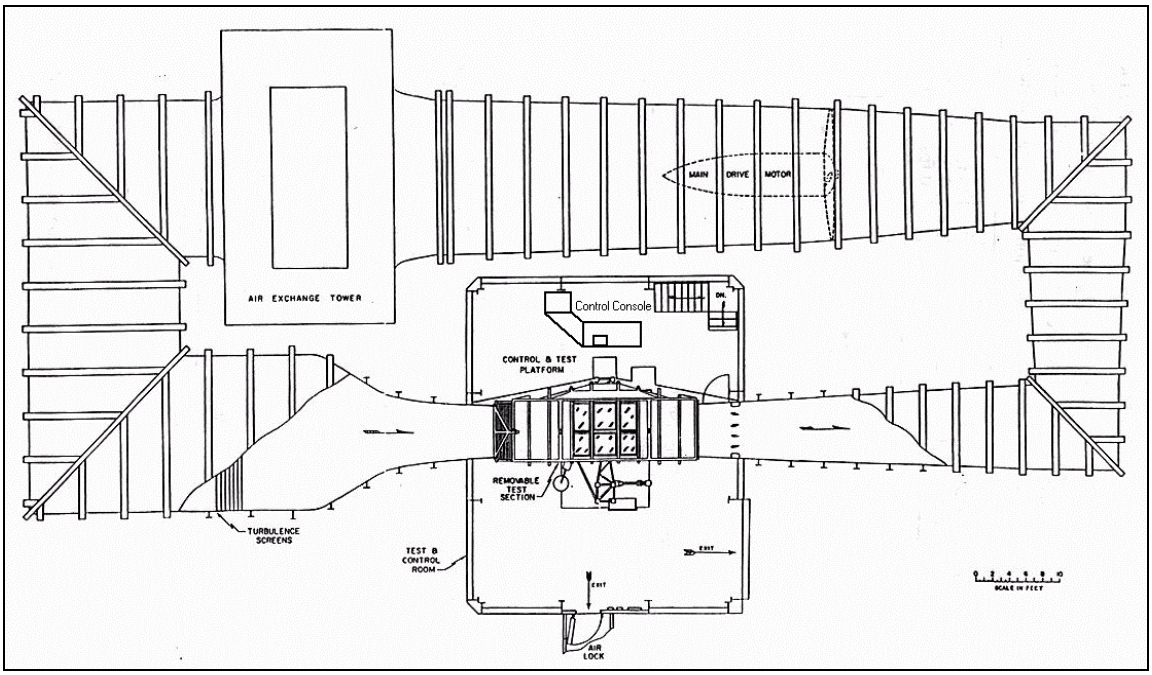

Figure 2.1: Top view of the Virginia Tech Stability Wind Tunnel

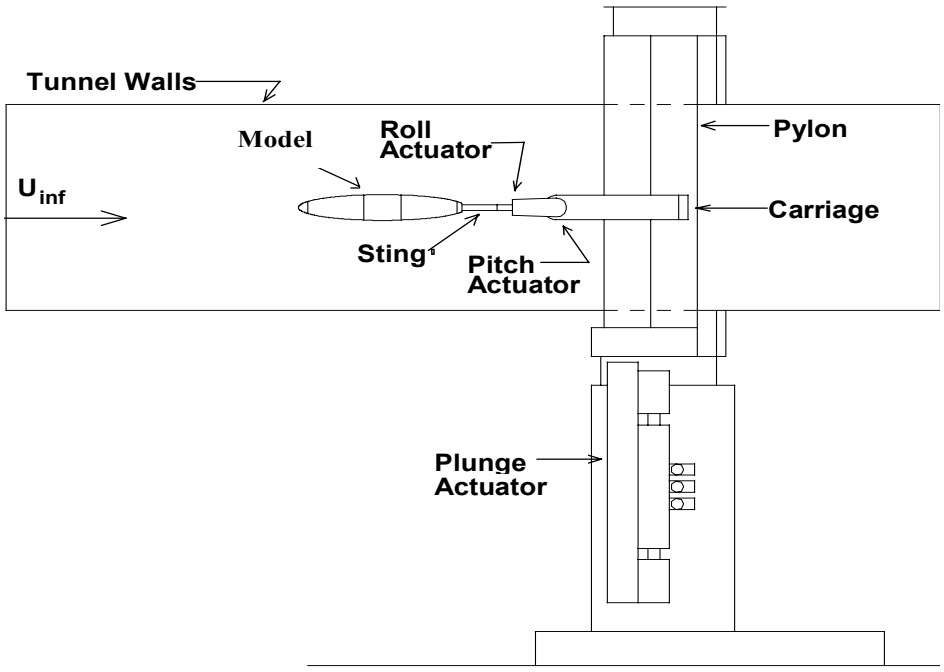

Figure 2.2: Dynamic Plunge-Pitch-Roll(DyPPiR) Model Mount installed in the wind tunnel.(taken from Wetzel [2])

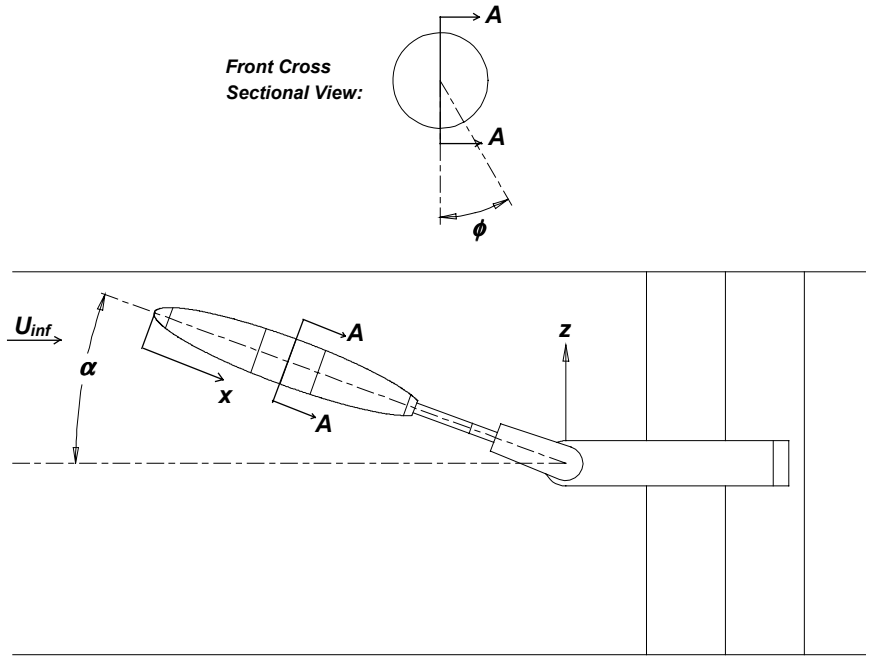

Figure 2.3: Coordinate nomenclature for the DyPPiR and the model. (taken from Wetzel [2])

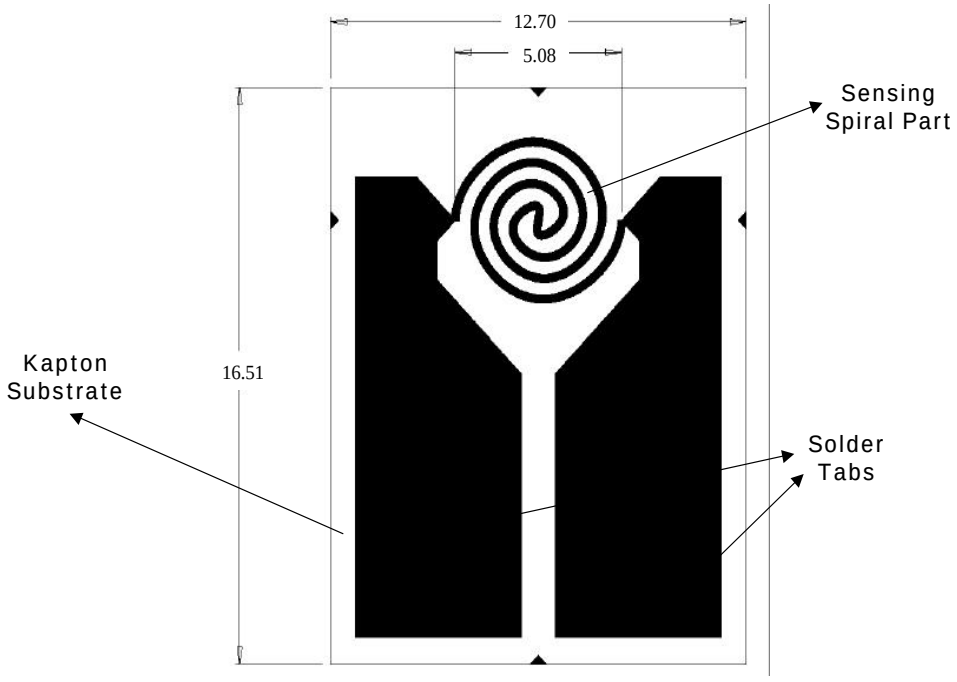

Figure 2.4: Hot-film sensor. All dimensions are in mm, and the figure is not drawn to scale.

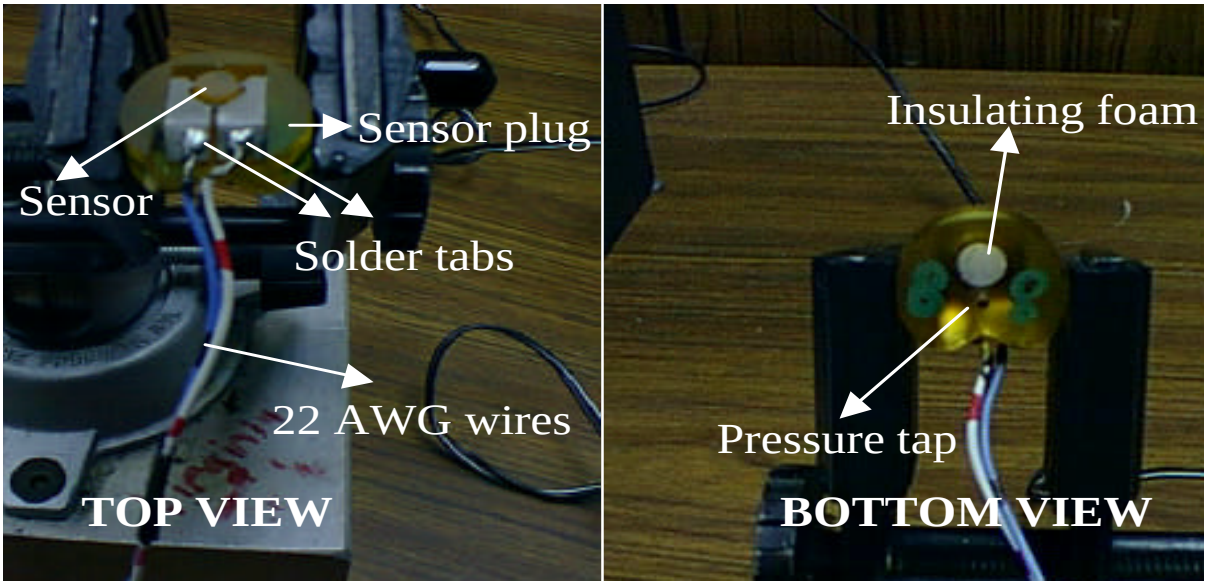

Figure 2.5: Sensor plug with a hot-film sensor mounted

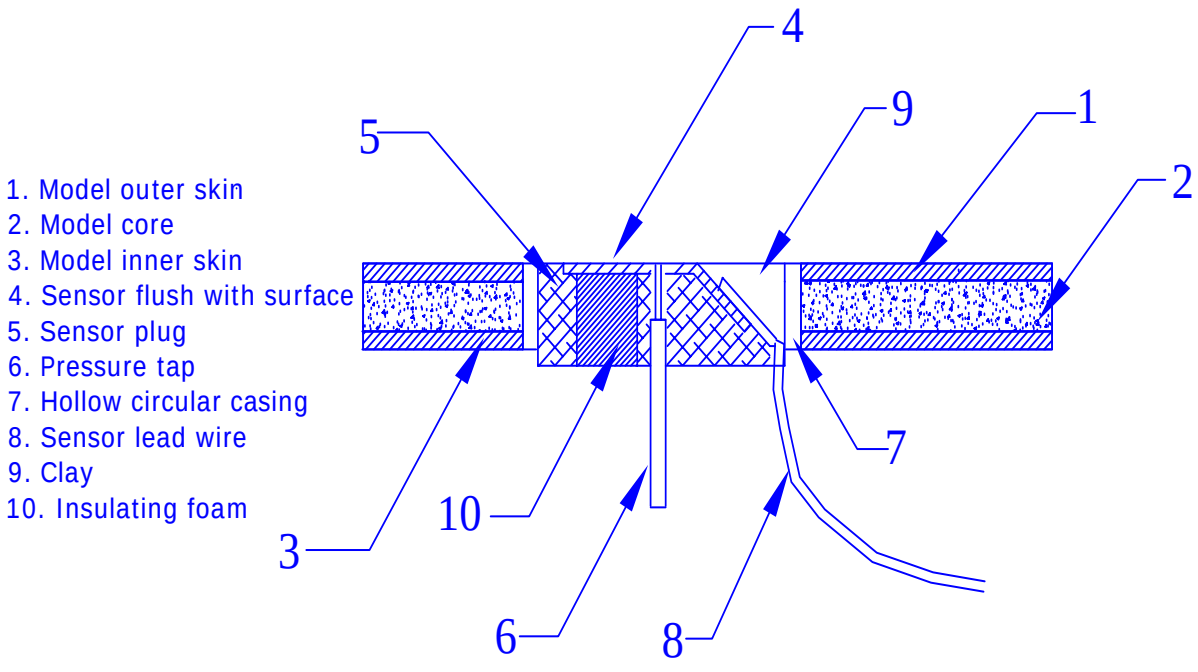

Figure 2.6: Schematic of the sensor mounting strategy

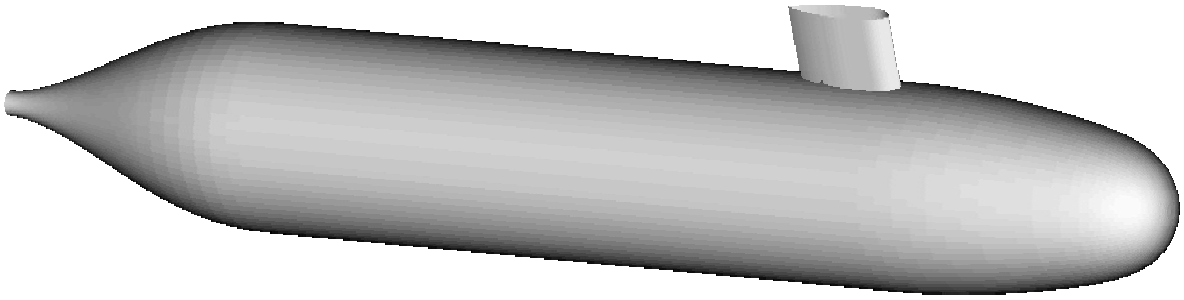

Figure 2.7: Computer generated 3-D view of the Suboff model with the sail

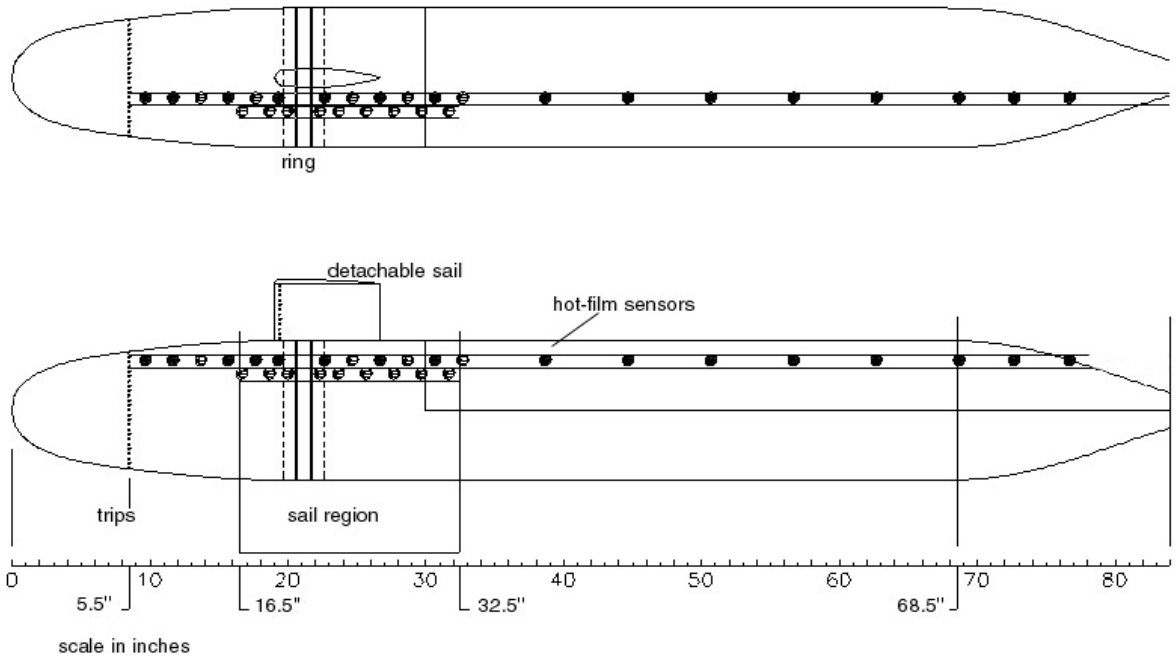

Figure 2.8: Top and side view of the model and the hot-film sensor locations

Figure 2.9: Barebody and sail-on-side configurations of the model